Cell. Mol. Life Sci. (2015) 72:2023–2039
DOI 10.1007/s00018-014-1798-6

Cellular and Molecular Life Sciences

RESEARCH ARTICLE

EW-7197 inhibits hepatic, renal, and pulmonary fibrosis by blocking TGF-β/Smad and ROS signaling

Sang-A Park · Min-Jin Kim · So-Yeon Park · Jung-Shin Kim · Seon-Joo Lee · Hyun Ae Woo · Dae-Kee Kim · Jeong-Seok Nam · Yhun Yhong Sheen

Received: 15 August 2014 / Revised: 27 November 2014 / Accepted: 1 December 2014 / Published online: 9 December 2014

Abstract Fibrosis is an inherent response to chronic damage upon immense apoptosis or necrosis. Transforming growth factor-beta1 (TGF-β1) signaling plays a key role in the fibrotic response to chronic liver injury. To develop anti-fibrotic therapeutics, we synthesized a novel small-molecule inhibitor of the TGF-β type I receptor kinase (ALK5), EW-7197, and evaluated its therapeutic potential in carbon tetrachloride (CCl_4) mouse, bile duct ligation (BDL) rat, bleomycin (BLM) mouse, and unilateral ureteral obstruction (UUO) mouse models. Western blot, immunofluorescence, siRNA, and ChIP analysis were carried out to characterize EW-7197 as a TGF-β/Smad signaling inhibitor in LX-2, Hepa1c1c7, NRK52E, and MRC5 cells. In vivo anti-fibrotic activities of EW-7197 were examined by microarray, immunohistochemistry, western blotting, and a survival study in the animal models. EW-7197 decreased the expression of collagen, α-smooth muscle actin (α-SMA), fibronectin, 4-hydroxy-2, 3-nonenal, and integrins in the livers of CCl_4 mice and BDL rats, in the lungs of BLM mice, and in the kidneys of UUO mice. Furthermore, EW-7197 extended the lifespan of CCl_4 mice, BDL rats, and BLM mice. EW-7197 blocked the TGF-β1-stimulated production of reactive oxygen species (ROS), collagen, and α-SMA in LX-2 cells and hepatic stellate cells (HSCs) isolated from mice. Moreover, EW-7197 attenuated TGF-β- and ROS-induced HSCs activation to myofibroblasts as well as extracellular matrix accumulation. The mechanism of EW-7197 appeared to be blockade of both TGF-β1/Smad2/3 and ROS signaling to exert an anti-fibrotic activity. This study shows that EW-7197 has a strong potential as an anti-fibrosis therapeutic agent via inhibition of TGF-β-/Smad2/3 and ROS signaling.

Keywords ALK5 inhibitor · CCl_4 hepatic fibrosis · BDL hepatic fibrosis · UUO renal fibrosis · BLM pulmonary fibrosis

Abbreviations

4-HNE	4-Hydroxy-2,3-nonenal
α-SMA	Alpha-smooth muscle actin
ALK5	Activin receptor-like kinase 5
BDL	Bile duct ligation
BLM	Bleomycin
CCl_4	Carbon tetrachloride
ECM	Extracellular matrix
EW-7197	*N*-[[4-([1,2,4]Triazolo[1,5-*a*]pyridin-6-yl)-5-(6-methylpyridin-2-yl)-1*H*-imidazol-2-yl]methyl]-2-fluoroaniline
GOx	Glucose oxidase
HSCs	Hepatic stellate cells
IHC	Immunohistochemistry
NOX	Nicotinamide adenine dinucleotide phosphate oxidase
Prdx	Peroxiredoxin

S.-A. Park and M.-J. Kim contributed equally to this work.

Electronic supplementary material The online version of this article (doi:10.1007/s00018-014-1798-6) contains supplementary material, which is available to authorized users.

S.-A. Park · M.-J. Kim · S.-Y. Park · J.-S. Kim · S.-J. Lee · H. A. Woo · D.-K. Kim · Y. Y. Sheen (✉)
College of Pharmacy, Ewha Womans University, Seodaemun-gu, Seoul 120-750, South Korea
e-mail: yysheen@ewha.ac.kr

J.-S. Nam
Laboratory of Tumor Suppressor, Lee Gil Ya Cancer and Diabetes Institute, Gachon University, Incheon 406-840, South Korea

qRT-PCR	Quantitative real-time reverse-transcriptase polymerase chain reaction
ROS	Reactive oxygen species
TGF-β	Transforming growth factor-beta
UUO	Unilateral ureteral obstruction

Introduction

Fibrosis enhances the deposition of extracellular matrix (ECM) proteins produced by myofibroblasts, resulting in distorted tissue architecture and organ failure [1–3]. Transforming growth factor-beta (TGF-β) is associated with stimulation of ECM production, reactive oxygen species (ROS) generation, and myofibroblast activation, which are the major events in tissue fibrosis [4, 5]. The production of collagen and α-smooth muscle actin (α-SMA), which are common hallmarks of fibrotic disease, is mediated by profibrotic cytokines and their intracellular signaling pathways, especially TGF-β-mediated Smad activation and ROS signaling [5, 6]. TGF-β signaling is activated by binding of TGF-β to the TGF-β type II receptor. Initially, this binding facilitates activation of the TGF-β type I receptor, also called activin receptor-like kinase 5 (ALK5), which contains a kinase domain that phosphorylates the cellular substrates Smad2/3. Phosphorylated Smad2/3 combines with Smad4 to form a heteromeric complex that translocates into the nucleus and regulates gene expression by binding to the promoters of its target genes [7]. In addition to the canonical Smad pathway, other pathways have been implicated in the transduction and regulation of TGF-β signaling [8]. However, the molecular mechanisms connecting Smad-independent pathways to the TGF-β receptor signaling complex remain elusive. TGF-β stimulates ROS generation by various mechanisms, resulting in up-regulation of profibrotic gene expression. ROS stimulate the activation of hepatic stellate cells (HSCs) and the production of type I collagen, which act as a mediator of TGF-β. Because oxidative stress causes pathological wound healing and leads to fibrosis, inhibitors of ROS generation typically have antifibrotic effects [9]. Based on these data, TGF-β signaling is a potential target for the prevention and treatment of fibrotic diseases, and direct inhibition of ALK5 shows potential in the prevention of detrimental profibrotic effects of TGF-β. Various agents that are capable of blocking the TGF-β signals, including antibodies and soluble receptors, have been tested as treatments for fibrosis in animal models [10–13]. Recently, synthetic inhibitors of ALK5 have been shown to specifically inhibit the effects of TGF-β in cellular assays [14–21]. However, their activities in animal fibrosis models are still unknown. Orally bioavailable small-molecule ALK5 inhibitors may overcome the limitations of tissue penetration and the delivery issues of antibody therapies. Because small-molecule inhibitors of ALK5, including SB-431542 [14], SB-505124 [15], SD-093 [16], SD-208 [17], LY-580276 [18], GW6604 [19], LY2157299 [20], and EW-7195 [21], were devised to directly block the catalytic activity of ALK5, they act as competitive inhibitors of the ATP-binding site in ALK5. Thus far, the ALK5 inhibitor GW6604 has shown anti-fibrotic effects at a dose of 80 mg/kg, bid, in a dimethylnitrosamine (DMN)-induced rat liver fibrosis model [19]. However, there is no proven drug for treatment of liver fibrosis patients [2, 12]. Recently, we reported that a novel small-molecule inhibitor of ALK5, EW-7197, shows high specificity and selectivity, and little toxicity [22].

In this study, we show that EW-7197 inhibits TGF-β/Smad and ROS signaling to exert its anti-fibrotic activity. EW-7197 inhibits the activation of HSCs and the deposition of collagen and α-SMA both in vitro and in vivo including carbon tetrachloride (CCl_4) mouse, bile duct ligation (BDL) rat, unilateral ureteral obstruction (UUO) mouse, and bleomycin (BLM) mouse models. Furthermore, EW-7197 showed low toxicity in a 4-week toxicity study of rats when administered at up to 120 mg/kg, qd. Additionally, EW-7197 (1.25, 2.5, or 5 mg/kg, qd) prolonged the lifespan of CCl_4 mice, BDL rats, and BLM mice. These data support that EW-7197 efficiently alleviates fibrosis in vivo and in vitro and might be a therapeutic option for treatment of tissue fibrosis.

Materials and methods

Reagents

N-[[4-([1,2,4]Triazolo[1,5-*a*]pyridin-6-yl)-5-(6-methylpyridin-2-yl)-1*H*-imidazol-2-yl]methyl]-2-fluoroaniline (EW-7197) [22] and LY2157299 were synthesized by Dr. D.K. Kim (Ewha Womans University, Seoul, Korea). Rotenone, diphenyleneiodonium (DPI), catalase, and *N*-acetylcysteine (NAC) were purchased from Sigma-Aldrich (St Louis, MO, USA). Recombinant human TGF-β1 was purchased from R&D Systems (Minneapolis, MN, USA) and 2 ng/ml of TGF-β1 was used in vitro experiments because in preliminary experiments it showed TGF-β responsiveness. CCl_4 was purchased from Duksan Pure Chemical (Seoul, Korea) and BLM sulfate was purchased from MB cell (Los Angeles, CA, USA).

Cell culture and transfection

LX-2 immortalized human activated HSCs were supplied by Dr. S.G. Kim (Seoul National University, Seoul, Korea). Hepa1c1c7 mouse hepatocytes, NRK-52E rat renal

proximal tubular cells, LX-2 cells, and 3TP-Lux stably transfected HaCaT cells (HaCaT-3TP-Lux) [21] were maintained in Dulbecco's modified Eagle's medium containing 10 % fetal bovine serum (FBS). MRC-5 human lung fibroblasts were maintained in minimum essential medium containing 10 % FBS. All media were purchased from Invitrogen (Carlsbad, CA, USA). Cells were maintained at 37 °C in a humidified incubator in the presence of 5 % CO_2. Mouse HSC-enriched cells and primary hepatocytes were obtained from normal C57BL/6 or *Prx* $I^{-/-}$ mouse livers by collagen perfusion methods (see below). For ALK5 silencing, cells were transfected in six-well plates with 100 nM (final) antisense ALK5 (Bioneer, Daejeon, Korea) using Lipofectamine 2000 (Invitrogen) according to the manufacturer's protocol. On-target plus nontargeting (NT) small interfering (si)RNA (Bioneer) was used as a negative control (Supplementary Table S1). Expression levels of mRNA and protein were measured at 24 h after transfection.

Isolation of primary crude liver cells by collagen perfusion methods

Male normal C57BL/6 and *Prdx* $I^{-/-}$ mice were obtained from Dr. H.A. Woo (Ewha Womans University). Mouse HSC-enriched cells and primary hepatocytes were isolated from the livers of 6- to 7-week-old male mice weighing 20–25 g as described previously [23].

Animals, treatment and specimen collection

Male C57BL/6 mice and Sprague–Dawley (SD) rats were purchased from Orient Bio (Seoul, Korea). Mice and rats were housed at 5–7 animals per cage at room temperature with a 12-h light/dark cycle. A normal chow diet and water were provided ad libitum. All experimental procedures were approved by the Animal Care Committee of Ewha Womans University and complied with the NIH Guide for the Care and Use of Laboratory Animals (Institute of Laboratory Animal Resources, National Research Council, WA). Because treatment with 5 mg/kg EW-7197 every day for 5 days per week resulted in the maximal effect, we performed EW-7197 treatment at 0.625, 1.25, 2.5, or 5 mg/kg five times a week for 4 weeks to examine a possible dose relationship. EW-7197 was dissolved in an artificial gastric fluid formulation (Veh). Rats and mice were randomly divided into six groups for efficacy and survival models: Sham control + Veh, fibrosis + Veh, fibrosis + 0.625 mg/kg EW-7197 (EW, qd), fibrosis + 1.25 mg/kg EW, fibrosis + 2.5 mg/kg EW, fibrosis + 5 mg/kg EW ($n = \sim 10$). EW-7197 was administered five times a week for 4 weeks in the efficacy model. In other experiments, male 6-week-old SD rats were randomly divided into nine EW-7197 dose groups: 0, 5, 10, 20, 30, 40, 50, 60, and 120 mg/kg, qd. EW-7197 was administered orally five times a week for 4 weeks. At 5 h after the last EW-7197 administration, the animals were deeply anesthetized by an intraperitoneal injection of Zoletil/Rompun (2:1 mixture). The animals were exsanguinated via the axillary artery, followed by collection of sera and excision of the liver, spleen, kidneys, and lungs. The sera and tissues were immediately stored at −80 °C until use.

Immunohistochemistry (IHC)

Tissues were fixed and stained with hematoxylin and eosin. Masson's trichrome staining of collagen was performed to quantify the fibrosis area. For IHC analysis, deparaffinized sections were washed with phosphate-buffered saline (PBS) and then treated with 3 % hydrogen peroxide for 5 min. The sections were blocked with 10 % normal goat serum in Tris–HCl-buffered saline or horse serum in PBS for 1 h and then incubated with primary antibodies for 1 h at room temperature (Supplementary Table S2). After washing, the sections were incubated with appropriate secondary antibodies (biotin-conjugated IgG; Vector Laboratories, Burlingame, CA, USA) and then developed with a Vecta-Elite streptavidin-peroxidase kit (Vector Laboratories). The sections were counterstained with diluted hematoxylin and examined by light microscopy. The staining intensity was measured in four fields of every section and quantified morphometrically using Image J software.

Immunofluorescence

Cultured cells and animal tissues were fixed with a 4 % paraformaldehyde solution (pH 7.4), blocked in 5 % bovine serum albumin (BSA) or 1 % BSA with normal serum in 0.1 % Triton X-100, and then incubated with primary/secondary antibodies or Rhodamine Phalloidin (Cytoskeleton, Denver, CO, USA). The cells were then counterstained with 4′,6-diamidino-2-phenylindole (DAPI). Images were obtained by fluorescence microscopy at magnification of 200× or 400×, or using an LSM 510 META laser confocal microscopy system (Carl Zeiss, Jena, Germany) at a magnification of 400× or 800×.

Microarray analyses

Total RNA from $\sim 5 \times 5$ mm^3 tissue pieces (right lobe of liver) was isolated using Trizol reagent (Invitrogen) and purified with RNeasy columns (Qiagen, Valencia, CA, USA) according to the manufacturer's instructions. After purification, aliquots of the RNA samples from each group of mice were pooled ($n = 4$). Experiments were performed

on Affymetrix GeneChip Mouse Gene 1.0 ST arrays that cover 21,041 genes (RefSeq-Entrez gene count; Affymetrix, Santa Clara, CA, USA). Arrays were scanned using a GeneChip™ Scanner 3000 7G controlled by GeneChip® Operating Software (GCOS, Affymetrix). Microarray scan data were analyzed with GeneChip® Operating and Expression Console Software (Affymetrix) and GenPlex v3.0 (ISTECH, Goyang, Korea). To compare the results of separate hybridization experiments, the signal intensity of each gene from different arrays was normalized according to the total intensity of all the genes in each array. The corresponding normalized signals on different arrays were compared to determine the fold induction or reduction in the gene expression between samples.

RNA isolation and reverse transcription-polymerase chain reaction (RT-PCR) analyses

Total RNA from 5 × 5 mm^3 tissue pieces or cultured cells was isolated using Trizol reagent. cDNAs were synthesized from 2 μg of total RNA by M-MLV reverse transcriptase (Invitrogen) using random primer (Invitrogen) for 1 h at 37 °C. Synthesized cDNAs were subjected to PCR amplification using *Taq* polymerase (Promega, Madison, WI, USA) or SYBR green real-time qRT-PCR reagents (Applied Biosystems, Foster City, CA, USA). The primers used are listed in Table 1. Cycling conditions were 5 min of preincubation at 95 °C, and then 30 s of denaturation at 95 °C and 30–45 s of annealing at 57–61 °C for 23–40 cycles using a GenePro™ Thermal Cycler (Bioer, Hangzhou, China) or StepOne Real-Time PCR System (Applied Biosystems).

Western blot analysis

About 5 × 5 mm^3 tissue pieces and cultured cells were lysed in 10× the volume of RIPA buffer [50 mM Tris–HCl (pH 7.5), 150 mM NaCl, 1 mM EDTA, 0.1 % sodium dodecyl sulfate, 0.5 % sodium deoxycholate, 1 % NP-40, 50 mM NaF, 1 mM Na_3VO_4, 1 mM phenylmethylsulfonyl fluoride, and a protease inhibitor cocktail (Roche Diagnostics, Mannheim, Germany)] for 20 min on ice. The lysates were clarified by centrifugation at 15,700*g* at 4 °C for 20 min. The protein content of the lysates was determined using a bicinchoninic acid protein assay kit (Pierce, Rockford, IL, USA). Proteins (20–60 μg) were separated by 6–12 % sodium dodecyl sulfate-polyacrylamide gel electrophoresis and then transferred to nitrocellulose (Whatman, Middlesex, UK) or polyvinylidene fluoride membrane (Millipore, Billerica, MA, USA). The membranes were blocked in solutions of 5 % BSA or 5 % nonfat dry milk and then probed with appropriate antibodies at 4 °C overnight. Following three washes in Tris-buffered saline, the membranes were incubated with horseradish peroxidase-conjugated secondary antibody for 1 h. Proteins were detected using an enhanced chemiluminescence kit (GE Healthcare, Princeton, NJ). Band intensities were analyzed by a LAS-3000 densitometer (Fujifilm, Tokyo, Japan).

Chromatin immune precipitation (ChIP) assays

LX-2 cells were treated with EW-7197 or LY-2157299 in the absence or presence TGF-β1 for 3 h. The cells were then harvested and subjected to ChIP assay to analyze Smad4 on the upstream promoter region of the mouse *PAI-1* gene.

Measurement of intracellular reactive oxygen species formation

LX-2 cells were seeded in a 96-well plate and treated with various ROS scavengers, such as rotenone (1 nM), diphenyleneiodonium (100 nM), catalase (500 U/ml), *N*-acetylcysteine (5 mM), LY2157299 (50 nM), or EW-7197 (50 nM) in the presence of glucose oxidase (GOx) (5 mU/ml) for 18 h. In other experiments, LX-2 cells were pretreated with LY2157299 or EW-7197 for 10 min and then stimulated with TGF-β1 (2 ng/ml) for 20 min. After treatment, the cells were incubated with redox-sensitive dye, 2′,7′-dichlorofluorescein diacetate (DCFDA; Molecular Probes, Eugene, OR) for 20 min at 37 °C. Intracellular ROS generated by oxidation of DCFDA were measured at an excitation wavelength 488 nm and emission wavelength of 535 nm in a Gemini EM fluorescence plate reader (Molecular Devices, Munich, Germany).

Statistical analyses

Results are expressed as the mean ± standard error of the mean (SEM) or standard deviation (SD). Statistical comparisons were determined by one-way analysis of variance followed by the Dunnett's two-tailed post-hoc test (SPSS ver. 10.0; SPSS, Chicago, IL, USA). Values of $p < 0.05$, 0.01 or 0.001 were considered significant.

Results

EW-7197, blocks TGF-β1/Smad signaling

We investigated whether an ALK5 inhibitor blocked nuclear translocation of p-Smads by immunofluorescence. A potent and specific ALK5 inhibitor, EW-7197 [22, 24] suppressed TGF-β1-induced nuclear translocation of p-Smad2/3 in LX-2 HSCs more effectively than

Table 1 Primers for qRT-PCR and ChIP assay

	Forward	Reverse
Mouse		
α-sma	GACGCTGAAGTATCCGATAGAACACG	CACCATCTCCAGAGTCCAGCACAAT
Col-1a1	ACCTGTGTGTTCCCTACTCA	GACTGTTGCCTTCGCCTCTG
Fn	CAACAACCGGAATTACACC	GGTCTCGGAGCTGGGAGTAG
Gapdh	ATGTGTCCGTCGTGGATCTGA	TTGAAGTCGCAGGAGACAACC
HO-1	AAGCCGAGAATGCTGAGTTCA	GCCGTGTAGATATGGTACAAGGA
Nox1	CGCTCCCAGCAGAAGGTCGTGATTACCAAG	GGAGTGACCCCAATCCCTGCCCCAACCA
Nox2	TGCAGTGCTATCATCCAAGC	CTTTCTCAGGGGTTCCAGTG
Noxa1	CACTGCTTGGTCAAATGCC	TTCTCAGATGTCCGAGAGCC
Noxo1	CATCAGGAAGCTTGGGAAGA	AGGAGCTGGGATGAGTTCAG
Nox4	TCAGGACAGATGCAGATGCT	CTGGAAAACCTTCCTGCTGT
Nqo1	AGGATGGGAGGTACTCGAATC	AGGCGTCCTTCCTTATATGCTA
Nrf2	GCCCACATTCCCAAACAAGAT	CCAGAGAGCTATTGAGGGACTG
Rat		
α-sma	GTGATCACCATCGGGAATGA	CAGCAATGCCTGGGTACATG
Col-1a1	AACCCCAAGGAGAAGAAGCA	AGCGTGCTGTAGGTGAATCG
Fn	GCTTCAAGCTGGGTGTACGA	AAGTTGGTTGGGGGAGACAG
Gapdh	ACCACAGTCCATGCCATCAC	ACGGATACATTGGGGGTAGG
Human		
GAPDH	TGGCAAATTCCATGGCACCG	CGCCCCACTTGATTTTGGAGG
NOX1	AGATGAACAAGCGTGGCTTC	AGATTGAGGGGCAATTAACA
NOX4	TCTGTTGTGGACCCAATTCA	AGCTGATTGATTCCGCTGAG
ChIP assay		
COL-1 promoter	AAATTCTGCCCATGTCGGG	AAACTCTGGCTCGTTGTCTGC
PAI-1 promoter	CCTCCA ACCTCAGCCAGACAAG	CCCAGCCCAACAGCCACA

Fn fibronectin

LY2157299, an ALK5 inhibitor that is currently in clinical studies but does not have any reported effects on fibrosis (Fig. 1a). Western blot analysis showed that EW-7197 inhibited phosphorylation of Smad3 in LX-2, Hepa1c1c7, NRK52E, and MRC5 cells in vitro (Fig. 1b). We also examined the effect of EW-7197 on transactivation of TGF-β1 signaling in HaCaT 3TP-Lux cells. Luciferase activity was increased 65-fold following TGF-β1 treatment (2 ng/ml), and EW-7197 showed stronger inhibition of ALK5 than other ALK5 inhibitors (Supplementary Fig. S1a). Regulation of the expression of *PAI-1*, a profibrotic and TGF-β-responsive target gene, is mediated by Smad activation through ALK5 [25]. A ChIP assay was carried out to examine whether EW-7197 inhibit regulation of *PAI-1* transcription. We found that EW-7197 inhibited transactivation of Smads on the promoter region of *PAI-1* (Fig. 1c). To confirm the specificity of EW-7197 in the inhibition of ALK5-mediated phosphorylation of Smad3, an ALK5 knockdown experiment using siRNA was carried out in LX-2 and Hepa1c1c7 cells. Compared with NT siRNA, ALK5 gene expression was effectively decreased by ALK5 siRNA (Supplementary Fig. S1b). The TGF-β1-induced Smad3 phosphorylation was almost completely abolished in cells that were transfected with ALK5 siRNA compared with that in cells transfected with NT siRNA (Fig. 1d). These results confirm that EW-7197 inhibited the ALK5-dependent phosphorylation of Smad3. In contrast, EW-7197 did not inhibit TGF-β1-induced phosphorylation of Smad1/5/8 in LX-2 and Hepa1c1c7 cells (Supplementary Fig. S1c). These results showed that targeting ALK5 by EW-7197 selectively inhibited TGF-β/Smad2/3 signaling. EW-7197 also inhibited phosphorylation of Smad3 in CCl_4-, and BDL-induced fibrotic livers, UUO-induced fibrotic kidneys, and BLM-induced fibrotic lungs in vivo (Fig. 1e–h; Supplementary Figs. S1d–S1g).

EW-7197 ameliorates α-SMA and collagen accumulation in the fibrotic liver, kidney, and lung

The appearance of α-SMA-positive myofibroblasts is considered to be a key event in the progression of tissue fibrosis [26]. Because TGF-β is an important mediator of transdifferentiation, we assessed the accumulation of fibrogenic myofibroblasts by morphometric quantification of

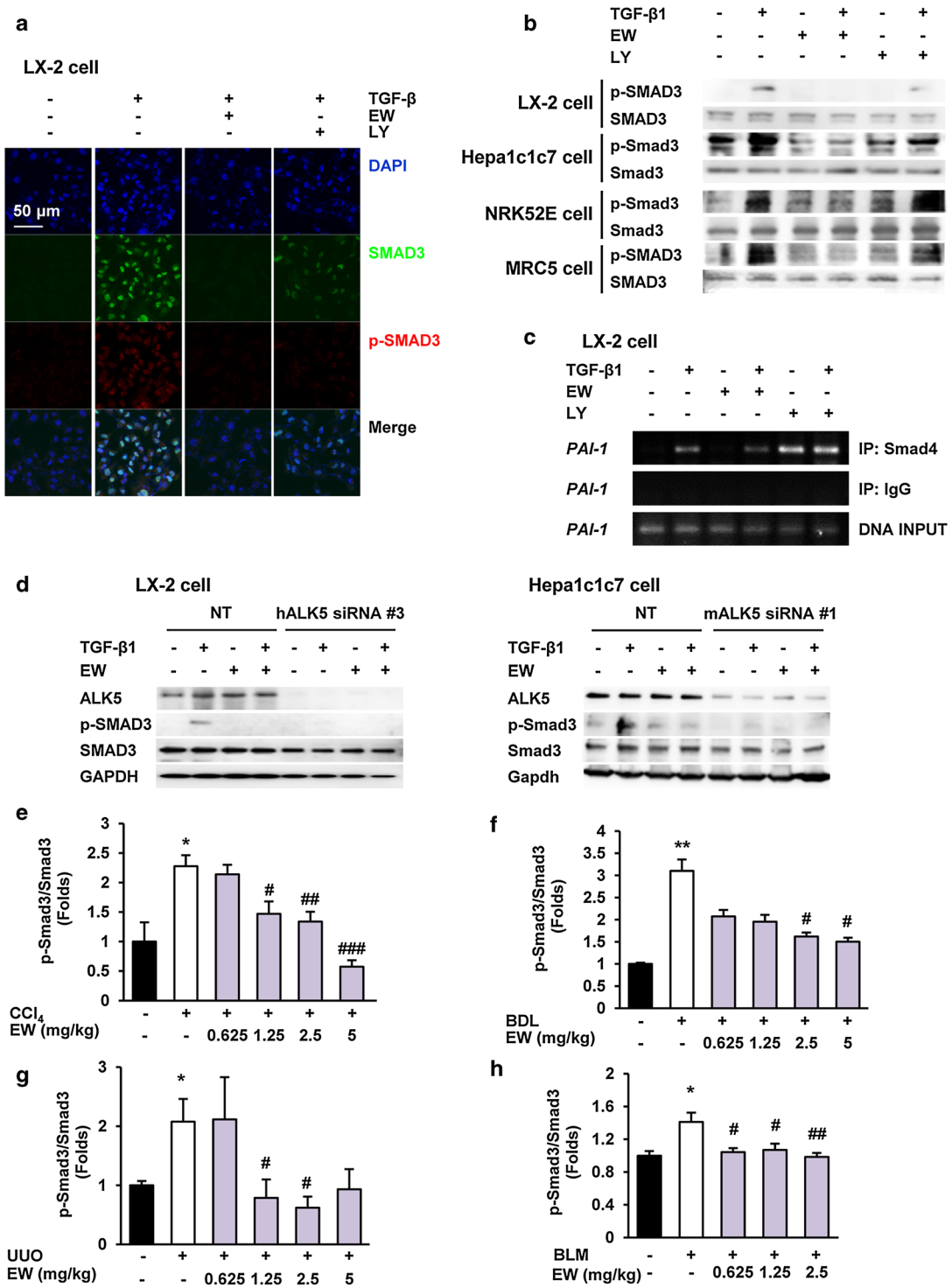

Fig. 1 The ALK5 inhibitor, EW-7197, blocks TGF-β1/Smad signaling. **a** Effects of EW-7197 (EW) and LY2157299 (LY) on nuclear translocation of p-Smad3 in LX-2 cells. LX-2 cells were treated with 0.5 μM of the indicated drug in the presence or absence of TGF-β1 (2 ng/ml) for 3 h. p-Smad3 and nuclei were stained with Alexa Flour 488 (*green*) and DAPI (*blue*), respectively. *Scale bars* 50 μm. **b** Effects of EW-7197 and LY2157299 on phosphorylation of Smad3 in LX-2, Hepa1c1c7, NRK52E, and MRC5 cells. Smad3 was used as a reference. **c** Effects of EW-7197 and LY2197299 on promoter activation of PAI-1 in LX-2 cells. **d** Effects of EW-7197 on phosphorylation of Smad3 in ALK5 siRNA-transfected LX-2 and Hepa1c1c7 cells. Smad3 and GAPDH were used as references. Densitometric analysis of western blot analysis of Smad3 phosphorylation in CCl_4 mice (**e**), BDL rats (**f**), UUO mice (**g**), BLM mice (**h**). Smad3 was used as a reference. $^{*}p < 0.05$ vs. Sham, $^{**}p < 0.01$ vs. Sham, $^{\#}p < 0.05$ vs. Vehicle, $^{\#\#}p < 0.01$ vs. Vehicle, $^{\#\#\#}p < 0.001$ vs. Vehicle

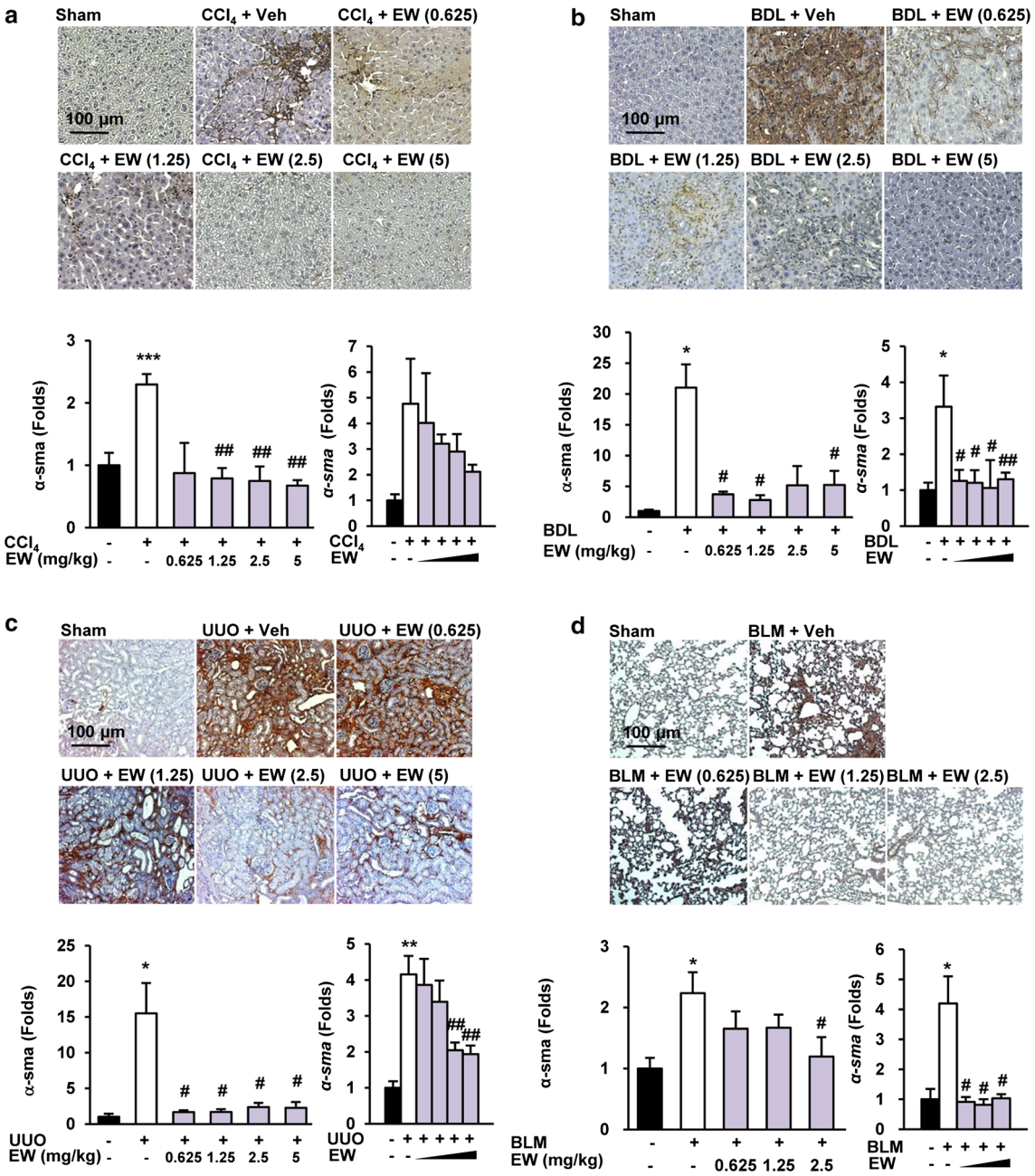

Fig. 2 EW-7197 ameliorates the accumulation of α-SMA in fibrotic tissue. **a**–**d** IHC (*upper*), western blot (*lower left*), and qRT-PCR (*lower right*) analysis of α-SMA in liver tissues of CCl_4 mice (**a**), BDL rats (**b**), UUO mice (**c**), and BLM mice (**d**). GAPDH was used as a reference. $^{*}p < 0.05$ vs. Sham, $^{**}p < 0.01$ vs. Sham, $^{***}p < 0.001$ vs. Sham, $^{\#}p < 0.05$ vs. Vehicle, $^{\#\#}p < 0.01$ vs. Vehicle. *Scale bars* 100 μm

α-SMA-positive cells. EW-7197 reduced α-SMA levels in the interstitial and tubular areas of liver tissues in both CCl_4 mice and BDL rats according to the IHC staining intensity. Moreover, EW-7197 decreased the elevated the protein and mRNA levels of α-SMA in CCl_4- and BDL-induced fibrotic livers (Fig. 2a, b; Supplementary Figs. S2a, S2b). In addition, EW-7197 treatment decreased the protein and mRNA levels of α-SMA in UUO mouse kidneys and BLM mouse lungs (Fig. 2c, d; Supplementary Fig. S2c, S2d). Tissue fibrosis, regardless of its cause, is characterized by rapid accumulation of ECM proteins, mainly collagen. To examine the anti-fibrotic effect of EW-7197, we measured collagen content as a marker of fibrosis. Histopathologically, EW-7197 treatment resulted in

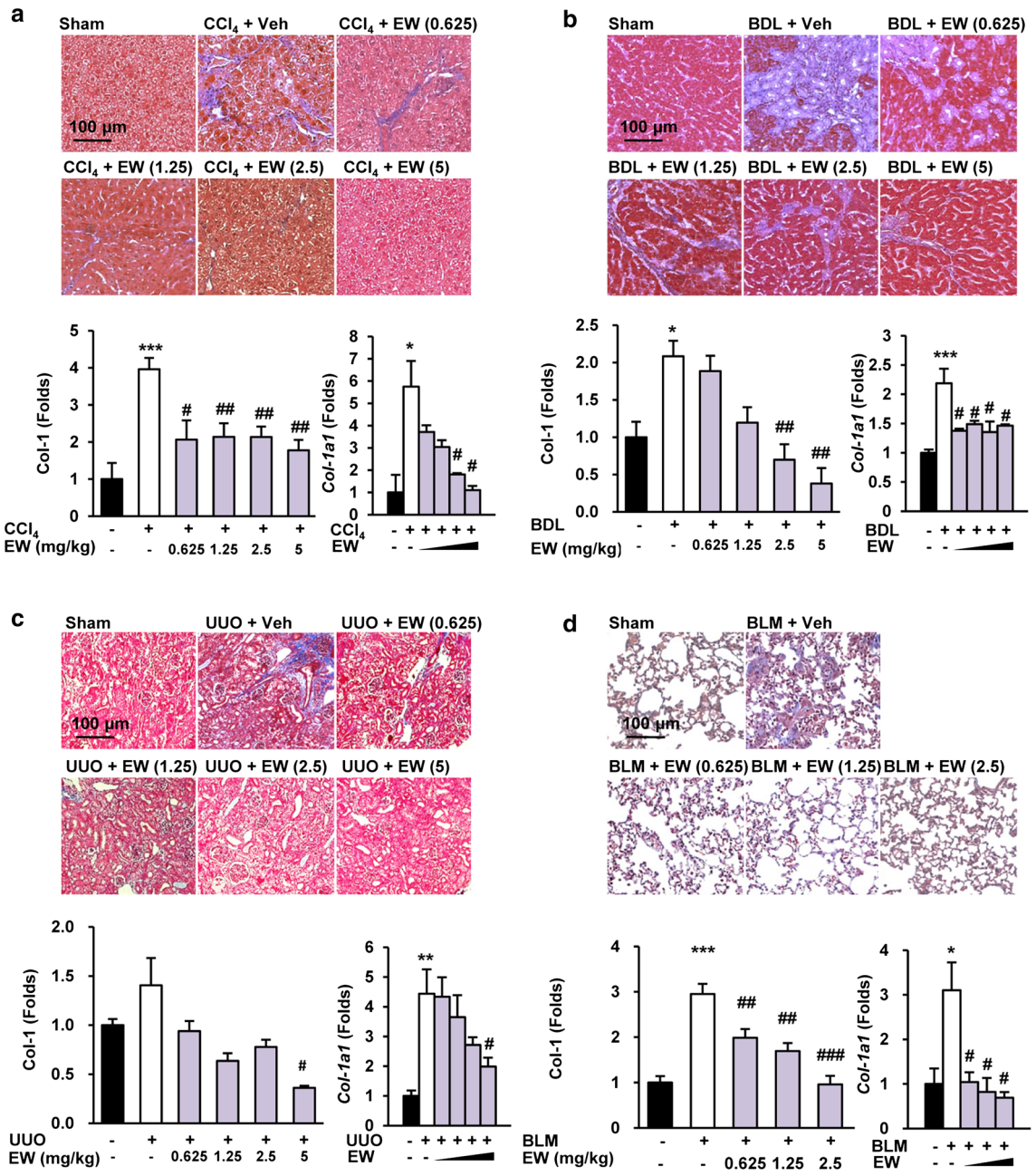

Fig. 3 EW-7197 ameliorates collagen accumulation in fibrotic tissue. **a**–**d** Masson's trichrome staining (*upper*), western blot (*lower left*), and qRT-PCR (*lower right*) analysis of collagen in liver tissues of CCl_4 mice (**a**), BDL rats (**b**), UUO mice (**c**), and BLM mice (**d**). GAPDH was used as a reference. $^{*}p < 0.05$ vs. Sham, $^{**}p < 0.01$ vs. Sham, $^{***}p < 0.001$ vs. Sham, $^{\#}p < 0.05$ vs. Vehicle, $^{\#\#}p < 0.01$ vs. Vehicle, $^{\#\#\#}p < 0.001$ vs. Vehicle. *Scale bars* 100 μm

dose-dependent inhibition of collagen accumulation in CCl_4 mouse and BDL rat livers, UUO mouse kidneys, and BLM mouse lungs based on Masson's trichrome staining (Fig. 3). Protein and mRNA levels of COL1A were also elevated in the fibrosis models and reduced by EW-7197 treatment (Fig. 3; Supplementary Fig. S3). Myofibroblasts express α_v integrins that may be critical for tissue fibrosis [27]. Therefore, we investigated the effect of EW-7197 on α_v integrin and fibronectin expression. EW-7197 reduced the increase in protein and mRNA levels of α_v integrin and fibronectin in CCl_4 mice, BDL rats, and UUO mice (Fig. 4; Supplementary Fig. S4). In BLM mice, there was no significant change in α_v integrin and fibronectin expression (data not shown).

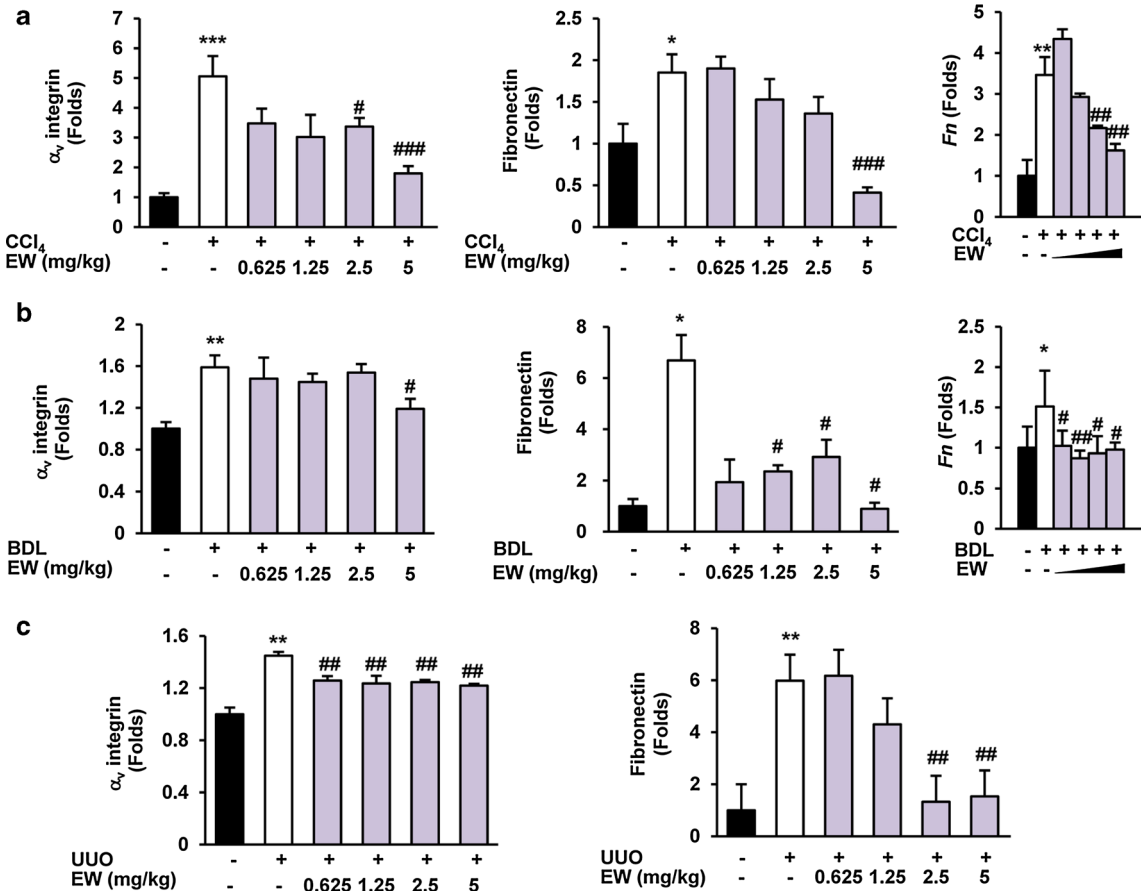

Fig. 4 EW-7197 decreases integrin and fibronectin expression in fibrotic tissue. **a**, **b** Protein expression levels of α_v integrin (*left*) and fibronectin (*middle*), and mRNA levels of fibronectin (*right*) in liver tissues of CCl_4 mice (**a**) and BDL rats (**b**). **c** Protein expression levels of integrin α_v (*left*) and fibronectin (*right*) in kidney tissues of UUO mice. GAPDH was used as a reference. $^{*}p < 0.05$ vs. Sham, $^{**}p < 0.01$ vs. Sham, $^{***}p < 0.001$ vs. Sham, $^{\#}p < 0.05$ vs. Vehicle, $^{\#\#}p < 0.01$ vs. Vehicle, $^{\#\#\#}p < 0.001$ vs. Vehicle

EW-7197 extends the lifespan and improves tissue function of fibrotic models

EW-7197 treatment did not affect healthy mice in terms of body weight and necroscopic observations (Table 2). Therefore, in vivo experiments exploring the anti-fibrotic efficacy of EW-7197 were performed without a sham-treated group with EW-7197 alone.

We investigated the effect of EW-7197 on the survival time of CCl_4 mice and found that both 1.25 and 2.5 mg/kg qd EW-7197 increased the survival of CCl_4 mice. In 2.5 and 1.25 mg/kg groups, 80 and 50 % of CCl_4 mice were still alive at 85 days after the start of treatment, respectively (Fig. 5a). We further investigated whether EW-7197 has a therapeutic effect on the CCl_4-induced fibrotic liver. We injected CCl_4 into mice twice per week, and EW-7197 treatment was started when development of liver fibrosis was confirmed by autopsy. EW-7197 extended the lifespan of the mice with liver fibrosis at dose of both 2.5 and 5 mg/kg (Fig. 5b). We examined whether EW-7197 prolonged the survival of BLM mice and BDL rats, and found that EW-7197 increased the survival of BLM mice (Fig. 5c). Up to 64 days, BDL rats treated with EW-7197 exhibited a significantly prolonged lifespan, although there was no statistically significant difference for the overall treatment period (Fig. 5d). In the in vivo experiments, there was no significant change in body weights (Tables 3, 4, 5, 6). These data showed that EW-7197 improved the lifespan of the fibrosis models without toxicity.

EW-7197 reduces oxidative stress

Oxidative stress is a major microenvironmental factor in the development of tissue fibrosis and a mediator of the fibrogenic effects of TGF-β [6, 28]. The aldehyde products of lipid peroxidation, such as 4-hydroxy-2,3-nonenal (4-HNE), have been implicated in the etiology of pathological changes under oxidative stress [28]. We found that 4-HNE elevation in CCl_4 mouse and BDL rat livers, the UUO mouse kidney, and BLM mouse lungs was inhibited by

Table 2 Effects of EW-7197 on body weight changes for 4 weeks oral repeat dose toxicity study in Sprague–Dawley rats

Groups (mg/kg)	Mean body weight (g)				Gain body weight change (%)
	Initial	Day 14	Day 21	Day 28	
0	200.9 ± 1.1	290.0 ± 6.7	322.0 ± 6.5	364.0 ± 5.5	81.2 ± 0.02
5	204.1 ± 1.6	275.0 ± 8.3	336.0 ± 8.6	356.5 ± 8.7	82.5 ± 0.04
10	205.8 ± 3.4	295.0 ± 5.0	360.0 ± 7.7	376.5 ± 8.1	83.0 ± 0.03
20	205.1 ± 3.0	295.0 ± 5.0	369.0 ± 7.1	388.5 ± 6.1	89.5 ± 0.03
30	199.9 ± 2.5	310.0 ± 10.0	347.0 ± 6.8	365.0 ± 6.1	82.5 ± 0.01
40	201.9 ± 1.3	290.0 ± 6.7	352.0 ± 6.8	371.0 ± 4.9	83.8 ± 0.02
50	205.4 ± 5.4	330.0 ± 8.2	357.0 ± 8.8	376.0 ± 8.7	83.5 ± 0.03
60	204.3 ± 1.8	325.0 ± 8.3	350.0 ± 6.3	373.5 ± 7.5	82.8 ± 0.03
120	184.4 ± 18.5	300.0 ± 7.5	340.0 ± 7.5	353.5 ± 8.4	81.9 ± 0.03

EW-7197 (0, 5, 10, 20, 30, 40, 50, 60, or 120 mg/kg, $n = 10$) dissolved in artificial gastric fluid formulation was given to rats orally five times per week for 4 weeks

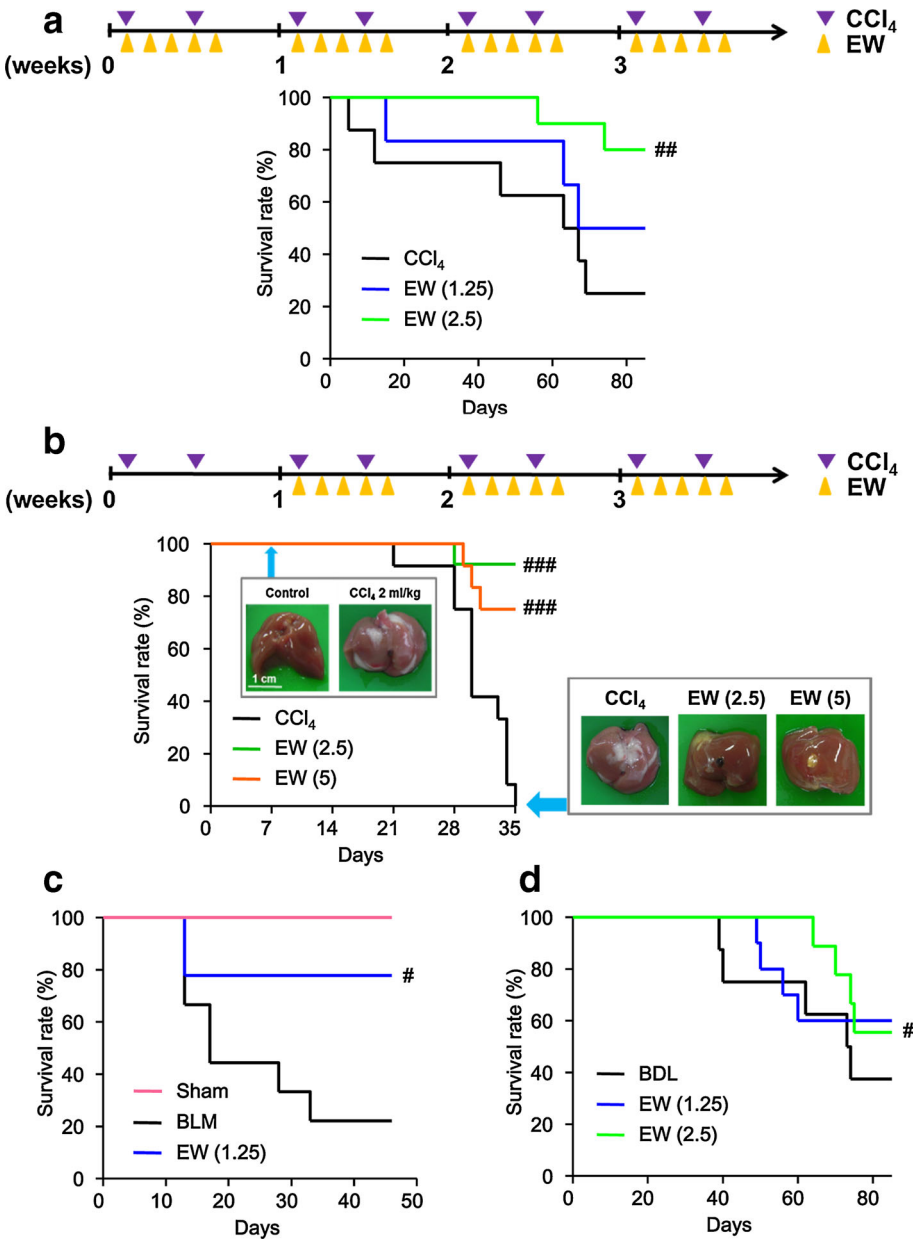

Fig. 5 EW-7197 extends the lifespan of CCl_4 mice, BDL rats, and BLM mice. **a**, **b** Kaplan–Meier plot of the overall survival of CCl_4 mice. *Arrows* indicate the start of EW-7197 treatment and the end of the experiment. *Scale bars* 1 cm. **c** Kaplan–Meier plot of the overall survival of BLM mice. **d** Kaplan–Meier plot of the overall survival of BDL rats. $^{\#}p < 0.05$ vs. Vehicle, $^{\#\#}p < 0.01$ vs. Vehicle, $^{\#\#\#}p < 0.001$ vs. Vehicle

Table 3 Effects of EW-7197 on body and organ weight changes in CCl_4 mice

Groups (mg/kg)	Body weight (g)	Organ weight	
		Liver/body (%)	Spleen/body (%)
Sham			
Veh	21.8 ± 0.6	4.25 ± 0.25	0.33 ± 0.02
CCl_4			
Veh	22.7 ± 0.5	5.54 ± 0.13***	0.43 ± 0.02*
EW (0.625)	21.3 ± 0.6	5.13 ± 0.20	0.34 ± 0.03#
EW (1.25)	21.9 ± 0.5	5.19 ± 0.19	0.39 ± 0.02
EW (2.5)	22.4 ± 0.5	5.30 ± 0.15	0.38 ± 0.02
EW (5)	22.4 ± 0.4	5.83 ± 0.16	0.41 ± 0.02

EW-7197 (EW: 0.625, 1.25, 2.5, or 5 mg/kg qd) dissolved in artificial gastric fluid formulation (Veh) was given to mice orally five times per week for 4 weeks following CCl_4 injection. The body and organ weights were determined 48 h after the last dosing. Data are expressed as means ± SEM

* $p < 0.05$ vs. Sham, *** $p < 0.005$ vs. Sham, # $P < 0.05$ vs. CCl_4 (ANOVA)

Table 4 Effects of EW-7197 on body and organ weight changes in BDL rats

Groups (mg/kg)	Body weight (g)	Organ weight	
		Liver/body (%)	Spleen/body (%)
Sham			
Veh	380.5 ± 11.2	3.12 ± 0.08	0.25 ± 0.01
BDL			
Veh	305.5 ± 8.5**	4.60 ± 1.04***	0.66 ± 0.06***
EW (0.625)	318.9 ± 11.4	3.99 ± 0.88	0.62 ± 0.09
EW (1.25)	302.5 ± 10.1	3.99 ± 0.96	0.49 ± 0.09
EW (2.5)	326.5 ± 6.9	3.46 ± 1.01	0.48 ± 0.12
EW (5)	327.5 ± 4.8#	3.25 ± 0.95	0.44 ± 0.09

EW-7197 (EW: 0.625, 1.25, 2.5, 5 mg/kg qd) dissolved in artificial gastric fluid formulation (Veh) was given to rats orally five times per week for 4 weeks following bile duct ligation (BDL). The body and organ weights were determined 48 h after the last dosing. Data are expressed as means ± SEM

** $p < 0.01$ vs. Sham, *** $p < 0.005$ vs. Sham, # $P < 0.05$ vs. BDL (ANOVA)

EW-7197 treatment (Fig. 6; Supplementary Fig. S5a). EW-7197 also reduced phosphorylation of p38 in CCl_4 mice (Supplementary Fig. S5b).

Nicotinamide adenine dinucleotide phosphate oxidase (NOX)-derived ROS facilitates TGF-β-mediated fibrosis by activation of myofibroblasts and accumulation of ECM proteins [9, 29]. Microarray analysis of CCl_4 mouse livers revealed alterations in the expression of many genes involved in ROS signaling (Fig. 7a). EW-7197 decreased up-regulation of the mRNA levels of NOX1, NOX2, and

Table 5 Effects of EW-7197 on body and organ weight changes in UUO mice

Groups (mg/kg)	Body weight (g)	Organ weight	
		L-Kidney/body (%)	Spleen/body (%)
Sham			
Veh	17.8 ± 0.2	0.73 ± 0.03	0.30 ± 0.02
UUO			
Veh	18.1 ± 0.3	3.01 ± 0.17***	0.53 ± 0.02*
EW (0.625)	18.4 ± 0.5	2.83 ± 0.16	0.43 ± 0.01###
EW (1.25)	18.2 ± 0.5	2.50 ± 0.15#	0.47 ± 0.06
EW (2.5)	19.0 ± 0.3	2.41 ± 0.15#	0.46 ± 0.02##
EW (5)	19.1 ± 0.5	2.76 ± 0.12	0.43 ± 0.02##

EW-7197 (EW: 0.625, 1.25, 2.5, 5 mg/kg qd) dissolved in artificial gastric fluid formulation (Veh) was given to mice orally five times per week for 4 weeks following unilateral ureteral obstruction (UUO). The body and organ weights were determined 48 h after the last dosing. Data are expressed as means ± SEM

* $p < 0.05$ vs. Sham, *** $p < 0.005$ vs. Sham, # $p < 0.05$ vs. UUO, ## $p < 0.01$ vs. UUO, ### $p < 0.001$ vs. UUO (ANOVA)

Table 6 Effects of EW-7197 on body and organ weight changes in BLM mice

Groups (mg/kg)	Body weight (g)	Organ weight	
		Lung/body (%)	Spleen/body (%)
Sham			
Veh	21.5 ± 0.5	0.97 ± 0.13	0.26 ± 0.03
BLM			
Veh	20.7 ± 0.8	1.51 ± 0.11*	0.26 ± 0.02
EW (0.625)	21.2 ± 0.4	1.28 ± 0.13	0.27 ± 0.01
EW (1.25)	20.9 ± 0.4	1.18 ± 0.03#	0.24 ± 0.01
EW (2.5)	21.4 ± 0.5	1.12 ± 0.05#	0.24 ± 0.02

EW-7197 (EW: 0.625, 1.25, 2.5, or 5 mg/kg qd) dissolved in artificial gastric fluid formulation (Veh) was given to mice orally five times per week for 4 weeks following bleomycin (BLM) injection. The body and organ weights were determined 48 h after the last dosing. Data are expressed as means ± SEM

* $p < 0.05$ vs. Sham, # $p < 0.05$ vs. BLM (ANOVA)

NOX components as well as the protein levels of NOX1 and NOX2 in CCl_4 mouse livers (Fig. 7b, c; Supplementary Fig. S6a). However, EW-7197 treatment did not change the protein or mRNA levels of NOX4 in CCl_4 mouse livers (data not shown). In UUO mouse kidneys, EW-7197 decreased the elevation in protein levels of NOX4 (Fig. 7d; Supplementary Fig. S6b). In addition, EW-7197 reduced the increase in mRNA levels of NOX1 and NOX4 in LX-2 cells (Fig. 7e). We detected the expression of NOX1 and NOX4 in LX-2 cells by immunofluorescence. TGF-β1 increased the expression of NOX1 and NOX4, which was inhibited by EW-7197. However,

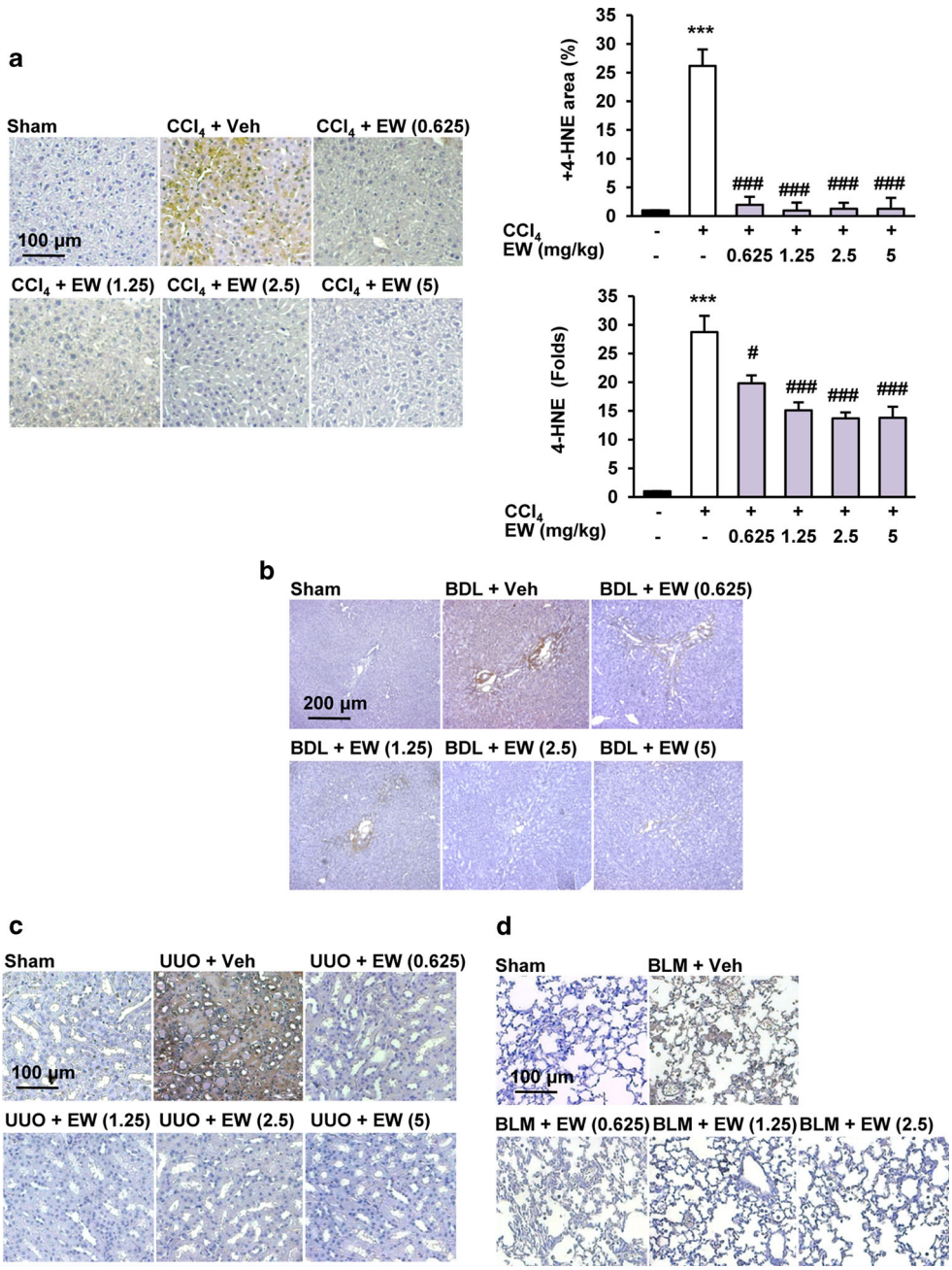

Fig. 6 EW-7197 reduces lipid peroxidation. **a** IHC staining of 4-HNE and densitometric analysis of IHC staining (*upper panel*) and western blots (*lower panel*) of liver tissues in CCl_4 mice. GAPDH was used as a reference. $^{***}p < 0.001$ vs. Sham, $^{\#}p < 0.05$ vs. CCl_4, $^{\#\#\#}p < 0.001$ vs. CCl_4. **b** IHC staining of 4-HNE in liver tissues of BDL rats. **c** IHC staining of 4-HNE in kidney tissues of UUO mice. **d** IHC staining of 4-HNE in lung tissues of BLM mice. *Scale bars* 100 μm (**a**, **c**, **d**); 200 μm (**b**)

treatment with LY2157299 had almost no effect in LX-2 cells (Fig. 7f). Taken together, ALK5 inhibition by EW-7197 reduced oxidative stress both in vivo and in vitro.

EW-7197 attenuates TGF-β- and ROS-induced HSC activation and ECM accumulation

To investigate the effect of ALK5 inhibition by EW-7197 on ROS level, we assessed ROS generation in DCFDA-loaded HSCs. Treatment with TGF-β1 significantly increased DCF fluorescence in LX-2 cells, which was comparable to the effect observed upon treatment with GOx. EW-7197 suppressed TGF-β1-induced intracellular ROS levels in LX-2 cells more effectively than LY2157299. Interestingly, EW-7197 also inhibited GOx-induced ROS level (Fig. 8a). These results indicated that EW-7197 not only inhibits ROS generation via inhibition of TGF-β1-induced NOX expression, but also eliminates ROS that occur independently of TGF-β signaling. Both TGF-β and ROS play key roles in the pathogenesis of liver fibrosis by activation of HSCs and production of ECM proteins including collagen [2, 6]. Immunofluorescence staining showed that both TGF-β1 and GOx stimulated the expression of α-SMA, filamentous actin, and collagen in

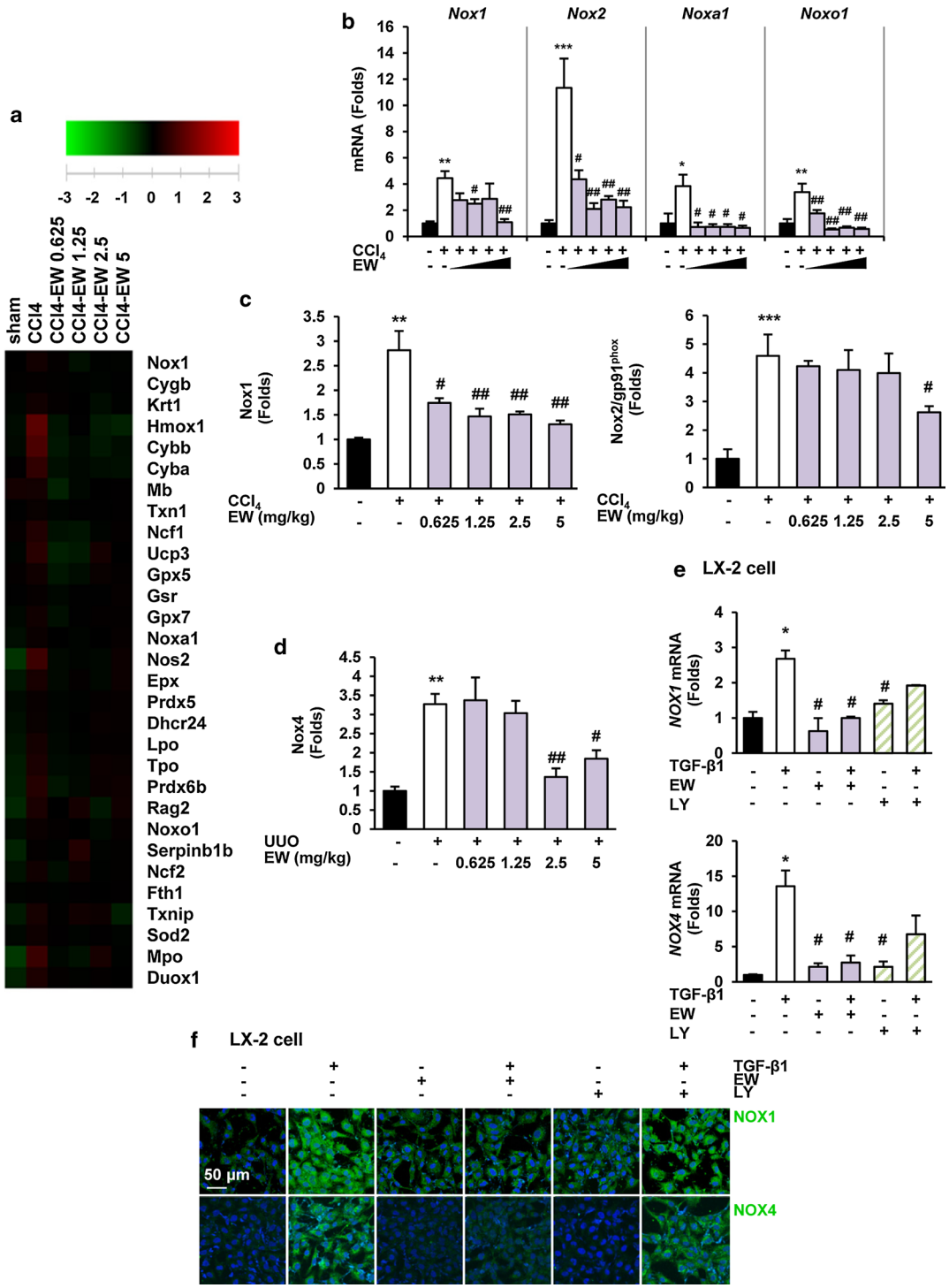

Fig. 7 EW-7197 attenuates TGF-β-induced NOX expression. **a** Heat maps depicting mRNA expression of oxidative stress-related genes in liver tissues of CCl_4 mice ($n = 4$). Gene expression levels are presented as the log2 ratio to the mean intensity and depicted as *color* variation from red (high expression) to green (low expression). **b** mRNA expression levels of NOXs and NOX components in liver tissues of CCl_4 mice. **c** Densitometric analysis of western blots of NOX1 and NOX2 in liver tissues of CCl_4 mice. **d** Densitometric analysis of western blots of NOX4 in kidney tissues of UUO mice. GAPDH was used as a reference. $^{*}p < 0.05$ vs. Sham, $^{**}p < 0.01$ vs. Sham, $^{***}p < 0.001$ vs. Sham, $^{\#}p < 0.05$ vs. Vehicle, $^{\#\#}p < 0.01$ vs. Vehicle. **e** mRNA expression levels of NOX1 (*upper*) and NOX4 (*lower*) in LX-2 cells. LX-2 cells were treated with the indicated drugs in the presence or absence of TGF-β1 for 24 h. GAPDH was used as a reference. $^{*}p < 0.05$ vs. untreated control, $^{\#}p < 0.05$ vs. TGF-β-treated control. **f** Immunofluorescence staining of NOX1 and NOX4 in LX-2 cells. Both NOX1 and NOX4 were stained with Alexa Flour 488 (*green*) and images were merged. *Scale bars* 50 μm

LX-2 cells. Treatment with EW-7197 and ROS scavengers led to similar reductions in TGF-β1- and GOx-induced expression of α-SMA, filamentous actin, and collagen levels in LX-2 cells (Fig. 8b, c). These data showed that ALK5 inhibition by EW-7197 inhibits the TGF-β- and/or ROS-induced activation of HSCs and accumulation of ECM proteins. Peroxiredoxin (Prdx) expression is induced by oxidative stress, and its induction is faster and more sensitive than that of other antioxidants. Therefore, Prdx is considered to be the most efficient protector against oxidative stress [30]. We observed that Prdx I was greatly increased in CCl_4 mouse livers compared with that in sham-treated mouse livers (Supplementary Fig. S7a). We therefore investigated the possibility that Prdx I might be associated with CCl_4-induced liver fibrosis. EW-7197 reduced the protein level of Prdx I which was increased in CCl_4 mouse livers (Fig. 8d; Supplementary Fig. S7b). Nuclear factor-erythroid 2-related factor 2 (Nrf2) is a ROS-sensitive transcriptional factor of many antioxidant enzymes and stress-responsive proteins such as NAD(P)H:quinone oxidoreductase (NQO1), heme oxygenase-1 (HO-1), and Prdx I [31]. To determine whether ALK5 inhibition by EW-7197 regulates ROS-induced transcription, we analyzed the mRNA expression levels of Nrf2 and Nrf2-dependent enzymes (HO-1 and NQO1). In CCl_4 mouse livers, the increased mRNA expression levels of *Nrf2*, *Ho-1*, and *Nqo1* were decreased by EW-7197 treatment (Fig. 8e). The inhibitory effect of EW-7197 on ROS-sensitive genes may attenuate fibrosis in CCl_4 mice. Therefore, we investigated the effect of EW-7197 on the increased oxidative stress in *Prdx I*-deficient mice. In HSCs isolated from *Prdx I*-deficient mice, EW-7197 inhibited the induction of α-SMA and collagen expression that would otherwise be stimulated by either TGF-β- or GOx-treatment (Fig. 8f). This result suggested that Prdx I might be involved in the anti-fibrotic effect of ALK5 inhibition by EW-7197 in CCl_4 mouse livers.

Discussion and conclusions

Fibrosis is closely linked to wound healing and prevents tissues from dismantling when inflammation, apoptosis, and necrosis occur. Chronic tissue damage results in cellular scar tissue even after removal of the causative triggers [32, 33]. Mild fibrosis remains mostly asymptomatic, but its progression to cirrhosis is the major cause of fibrosis-related morbidity and mortality. Thus, there is an urgent need for anti-fibrotic drugs that prevent progression to cirrhosis [34–36]. TGF-β is the most potent primary inducer of fibrogenesis in various organs such as the kidney, heart, and lung [5]. TGF-β is associated with stimulation of ECM production, one of the major events in tissue fibrogenic progression [4, 5]. Based on these findings, TGF-β signaling appears to be a potential target for the prevention or treatment of fibrotic diseases, and direct inhibition of ALK5 might be an attractive approach to prevent the detrimental profibrotic effects of TGF-β. A small-molecule ALK inhibitor, GW6604, at a dose of 80 mg/kg, shows anti-fibrotic efficacy in DMN-induced liver fibrosis in vivo. However, GW6604 does not suppress the body weight loss of DMN-treated rats [19]. Conversely, in our study, EW-7197 extended the lifespan of various animal fibrosis models at a low dose (<5 mg/kg, qd). Although a long-term safety study is required to determine its toxicity profile, a preclinical 4-week-old rat study with EW-7197 at dose up to 120 mg/kg revealed little toxicity (Table 2). The maximum tolerated dosage of EW-7197 in rats appeared to be 50 mg/kg/day for males and 20 mg/kg/day for females. Based on kinase assay results, the IC_{50} value of GW6604 (140 nM) [19] is larger than that of EW-7197 (13 nM) [22]. Although it is difficult to compare the efficacy and toxicity of GW6604 with those of EW-7197 because of the differences in the animal models, EW-7197 appears to be a more potent anti-fibrotic agent than GW6604. TGF-β increases the generation of ROS that mediate many of the fibrotic effects of TGF-β and decreases the concentration of antioxidants such as glutathione and Prdxs, in various cell types [6, 28, 37, 38]. This study demonstrated that EW-7197 exerts an anti-fibrotic effect by inhibition of both canonical Smad and non-canonical ROS signaling pathway in CCl_4- and BDL-induced fibrotic liver, UUO-induced fibrotic kidney, and BLM-induced fibrotic lungs (Figs. 1, 2, 3, 4, 5, 6, 7). However, the molecular mechanisms connecting Smad-independent pathways to the TGF-β receptor signaling complex remain unclear and might involve crosstalk between ALK5 and other cellular signaling components.

Fig. 8 EW-7197 attenuates TGF-β- and ROS-induced HSC activation and ECM accumulation. **a** Representative images and measurement of intracellular ROS levels in LX-2 cells. Cells were treated with rotenone (1 nM, R), DPI (100 nM, D), catalase (500 U/ml, C), NAC (5 mM, N), LY2157299 (50 nM), or EW-7197 (50 nM). $^{***}p < 0.001$ vs. untreated control, $^{\#\#\#}p < 0.001$ vs. GOx-treated control. **b** Immunofluorescence staining of α-SMA and phalloidin in LX-2 cells. α-SMA and rhodamine phalloidin were stained with Alexa Flour 488 (*green*)- and 555 (*red*)-conjugated IgGs, respectively. **c** Immunofluorescence staining of COL1A in LX-2 cells. COL1A was stained with Alexa Flour 488 (*green*)-conjugated IgG and images were merged. *Scale bars* 50 μm. **d** Densitometric analysis of western blots of Prdx I in liver tissues of CCl_4 mice. **e** mRNA expression levels of *Nrf2, Ho-1* and *Nqo1* in liver tissues of CCl_4 mice. GAPDH was used as a reference. $^{**}p < 0.01$ vs. Sham, $^{***}p < 0.001$ vs. Sham, $^{\#}p < 0.05$ vs. CCl_4, $^{\#\#}p < 0.01$ vs. CCl_4, $^{\#\#\#}p < 0.001$ vs. CCl_4. **f** Effects of EW-7197 on GOx and TGF-β induced α-SMA and COL1A expression in the $Prdx1^{+/+}$ and $Prdx1^{-/-}$ mouse HSCs enriched cells. Cells were treated with EW-7197 in the presence or absence of GOx or TGF-β1 for 24 h. Ponceau S-stained membrane was used as reference

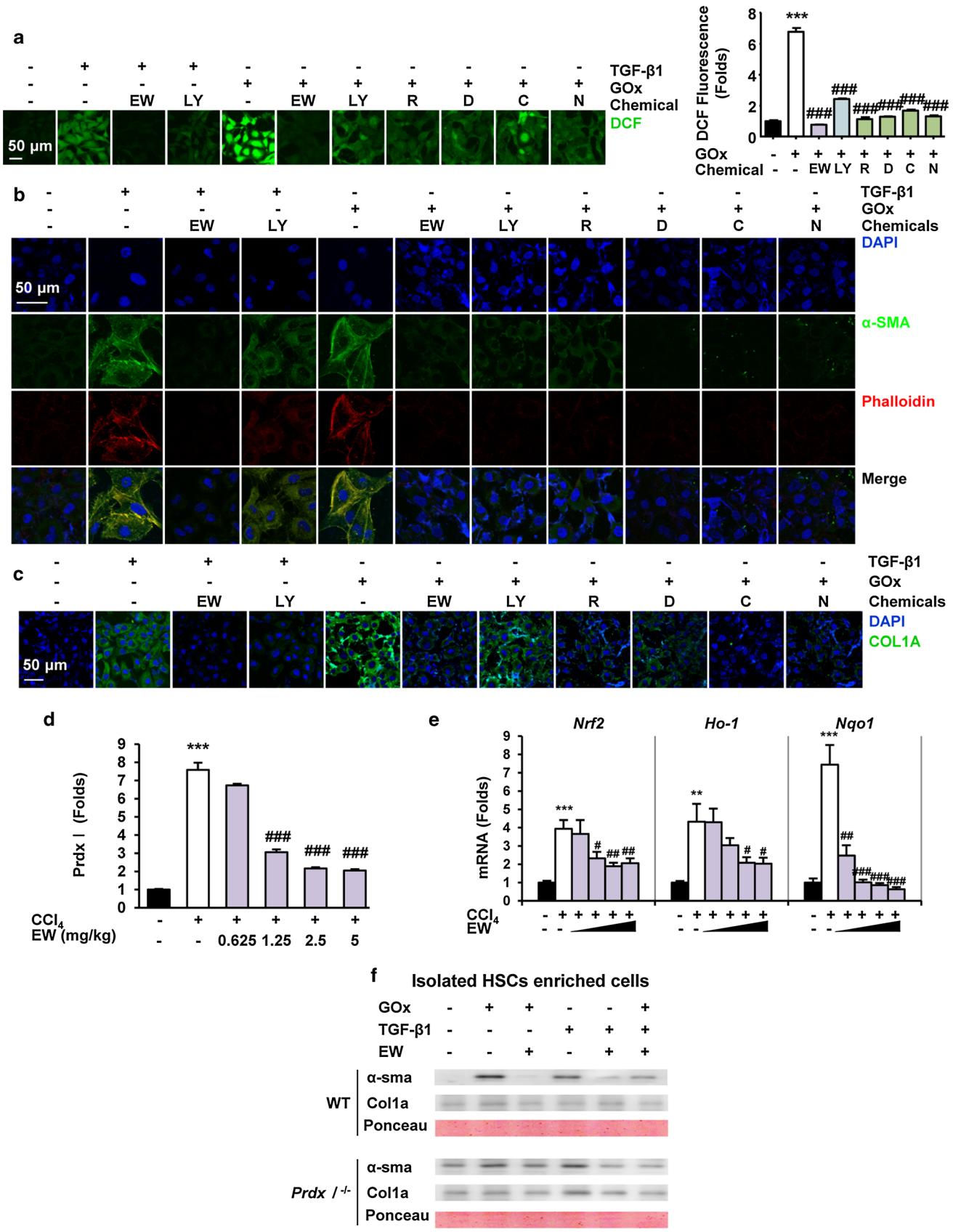
a
TGF-β1
GOx
Chemical
DCF
EW
LY
R
D
C
N
50 μm
DCF Fluorescence (Folds)
b
Chemicals
DAPI
α-SMA
Phalloidin
Merge
c
COL1A
d
Prdx I (Folds)
CCl4
EW (mg/kg)
0.625
1.25
2.5
5
e
Nrf2
Ho-1
Nqo1
mRNA (Folds)
f
Isolated HSCs enriched cells
α-sma
Col1a
Ponceau
WT
Prdx I -/-

Currently, EW-7197 is under a phase II clinical trial for breast cancer in the USA (US IND 119528). In this study, we found that EW-7197 has an anti-fibrotic efficacy in vitro and in vivo. This is the first report showing that a novel small-molecule ALK5 inhibitor prolongs the life-spans of CCl_4 mice, BDL rats, UUO mice, and BLM mice. Although further long-term studies are required to identify the optimal drug dosage, our studies provides a proof of concept for the use of the novel ALK5 inhibitor EW-7197 as a potential anti-fibrosis drug.

Acknowledgments This work was supported by the Korea Science and Engineering Foundation (KOSEF) grant, which is funded by the Korean government (MEST) (No. 20090093972). We thank Seung Won Kim, Sol-Ji Kim, Jung In Jee, and Min-Kyung Park for technical and administrative support.

Conflict of interest The authors have no conflicts of interest.

References

1. Schuppan D, Kim YO (2013) Evolving therapies for liver fibrosis. J Clin Investig 123(5):1887–1901
2. Bataller R, Brenner DA (2005) Liver fibrosis. J Clin Invest 115(2):209–218
3. Desmouliere A, Chaponnier C, Gabbiani G (2005) Tissue repair, contraction, and the myofibroblast. Wound Repair Regen 13(1):7–12
4. Friedman SL (2000) Molecular regulation of hepatic fibrosis, an integrated cellular response to tissue injury. J Biol Chem 275(4):2247–2250
5. Leask A, Abraham DJ (2004) TGF-β signaling and the fibrotic response. FASEB J 18(7):816–827
6. Liu R-M, Gaston Pravia K (2010) Oxidative stress and glutathione in TGF-β-mediated fibrogenesis. Free Radic Biol Med 48(1):1–15
7. Shi Y, Massagué J (2003) Mechanisms of TGF-β signaling from cell membrane to the nucleus. Cell 113(6):685–700
8. Derynck R, Akhurst RJ (2007) Differentiation plasticity regulated by TGF-β family proteins in development and disease. Nat Cell Biol 9(9):1000–1004
9. Samarakoon R, Overstreet JM, Higgins PJ (2013) TGF-β signaling in tissue fibrosis: redox controls, target genes and therapeutic opportunities. Cell Signal 25(1):264–268
10. Akhurst R, Hata A (2012) Targeting the TGFβ signalling pathway in disease. Nat Rev Drug Discov 11:790–811
11. Liu X, Hu H, Yin JQ (2006) Therapeutic strategies against TGF-β signaling pathway in hepatic fibrosis. Liver International 26(1):8–22
12. Lotersztajn S, Julien B, Teixeira-Clerc F, Grenard P, Mallat A (2005) Hepatic fibrosis: molecular mechanisms and drug targets. Annu Rev Pharmacol Toxicol 45:605–628
13. Wynn TA, Ramalingam TR (2012) Mechanisms of fibrosis: therapeutic translation for fibrotic disease. Nat Med 18(7):1028–1040
14. Hjelmeland MD, Hjelmeland AB, Sathornsumetee S, Reese ED, Herbstreith MH, Laping NJ, Friedman HS, Bigner DD, Wang X-F, Rich JN (2004) SB-431542, a small molecule transforming growth factor-β-receptor antagonist, inhibits human glioma cell line proliferation and motility. Mol Cancer Ther 3(6):737–745
15. Byfield SD, Major C, Laping NJ, Roberts AB (2004) SB-505124 is a selective inhibitor of transforming growth factor-β type I receptors ALK4, ALK5, and ALK7. Mol Pharmacol 65(3):744–752
16. Subramanian G, Schwarz RE, Higgins L, McEnroe G, Chakravarty S, Dugar S, Reiss M (2004) Targeting endogenous transforming growth factor β receptor signaling in SMAD4-deficient human pancreatic carcinoma cells inhibits their invasive phenotype 1. Cancer Res 64(15):5200–5211
17. Uhl M, Aulwurm S, Wischhusen J, Weiler M, Ma JY, Almirez R, Mangadu R, Liu Y-W, Platten M, Herrlinger U (2004) SD-208, a novel transforming growth factor β receptor I kinase inhibitor, inhibits growth and invasiveness and enhances immunogenicity of murine and human glioma cells in vitro and in vivo. Cancer Res 64(21):7954–7961
18. Sawyer T (2004) Novel oncogenic protein kinase inhibitors for cancer therapy. Curr Med Chem Anticancer Agents 4(5):449
19. Gouville AC, Boullay V, Krysa G, Pilot J, Brusq JM, Loriolle F, Gauthier JM, Papworth SA, Laroze A, Gellibert F (2005) Inhibition of TGF-β signaling by an ALK5 inhibitor protects rats from dimethylnitrosamine-induced liver fibrosis. Br J Pharmacol 145(2):166–177
20. Zhou L, McMahon C, Bhagat T, Alencar C, Yu Y, Fazzari M, Sohal D, Heuck C, Gundabolu K, Ng C (2011) Reduced SMAD7 leads to overactivation of TGF-β signaling in MDS that can be reversed by a specific inhibitor of TGF-β receptor I kinase. Cancer Res 71(3):955–963
21. Park C-Y, Son J-Y, Jin CH, Nam J-S, Kim D-K, Sheen YY (2011) EW-7195, a novel inhibitor of ALK5 kinase inhibits EMT and breast cancer metastasis to lung. Eur J Cancer 47(17):2642–2653
22. Jin CH, Krishnaiah M, Sreenu D, Subrahmanyam V, Rao K, Lee HJ, Park S-J, Park H-J, Lee K, Sheen YY (2014) Discovery of *N*-((4-([1, 2, 4] triazolo [1, 5-a] pyridin-6-yl)-5-(6-methylpyridin-2-yl)-1H-imidazol-2-yl) methyl)-2-fluoroaniline (EW-7197): a highly potent, selective, and orally bioavailable inhibitor of TGF-β type 1 receptor kinase as cancer immunotherapeutic/antifibrotic agent. J Med Chem 57:4213–4238
23. Taura K, Miura K, Iwaisako K, Österreicher CH, Kodama Y, Penz-Österreicher M, Brenner DA (2010) Hepatocytes do not undergo epithelial-mesenchymal transition in liver fibrosis in mice. Hepatology 51(3):1027–1036
24. Son JY, Park S-Y, Kim S-J, Lee SJ, Park S-A, Kim M-J, Kim SW, Kim D-K, Nam J-S, Sheen YY (2014) EW-7197, a novel ALK-5 kinase inhibitor, potently inhibits breast to lung metastasis. Mol Cancer Ther 0903:2013
25. Verrecchia F, Mauviel A (2007) Transforming growth factor-beta and fibrosis. World J Gastroenterol 13(22):3056–3062
26. Wynn T (2008) Cellular and molecular mechanisms of fibrosis. J Pathol 214(2):199–210
27. Henderson NC, Arnold TD, Katamura Y, Giacomini MM, Rodriguez JD, McCarty JH, Pellicoro A, Raschperger E, Betsholtz C, Ruminski PG (2013) Targeting of [alpha] v integrin identifies a core molecular pathway that regulates fibrosis in several organs. Nat Med 19(12):1617–1624
28. Poli G (2000) Pathogenesis of liver fibrosis: role of oxidative stress. Mol Aspects Med 21(3):49–98
29. Paik YH, Iwaisako K, Seki E, Inokuchi S, Schnabl B, Österreicher CH, Kisseleva T, Brenner DA (2011) The nicotinamide adenine dinucleotide phosphate oxidase (NOX) homologues NOX1 and NOX2/gp91phox mediate hepatic fibrosis in mice. Hepatology 53(5):1730–1741
30. Rhee SG, Chae HZ, Kim K (2005) Peroxiredoxins: a historical overview and speculative preview of novel mechanisms and emerging concepts in cell signaling. Free Radic Biol Med 38(12):1543–1552

31. Kensler TW, Wakabayashi N, Biswal S (2007) Cell survival responses to environmental stresses via the Keap1-Nrf2-ARE pathway. Annu Rev Pharmacol Toxicol 47:89–116
32. Issa R, Zhou X, Constandinou CM, Fallowfield J, Millward-Sadler H, Gaca MD, Sands E, Suliman I, Trim N, Knorr A (2004) Spontaneous recovery from micronodular cirrhosis: evidence for incomplete resolution associated with matrix cross-linking. Gastroenterology 126(7):1795–1808
33. Popov Y, Sverdlov DY, Sharma AK, Bhaskar KR, Li S, Freitag TL, Lee J, Dieterich W, Melino G, Schuppan D (2011) Tissue transglutaminase does not affect fibrotic matrix stability or regression of liver fibrosis in mice. Gastroenterology 140(5):1642–1652
34. Popov Y, Schuppan D (2009) Targeting liver fibrosis: strategies for development and validation of antifibrotic therapies. Hepatology 50(4):1294–1306
35. Friedman SL (2010) Evolving challenges in hepatic fibrosis. Nat Rev Gastroenterol Hepatol 7(8):425–436
36. Friedman SL, Sheppard D, Duffield JS, Violette S (2013) Therapy for fibrotic diseases: nearing the starting line. Sci Transl Med 5(167):167sr161
37. Basu S (2003) Carbon tetrachloride-induced lipid peroxidation: eicosanoid formation and their regulation by antioxidant nutrients. Toxicology 189(1):113–127
38. Kim K-Y, Choi I, Kim S-S (2000) Progression of hepatic stellate cell activation is associated with the level of oxidative stress rather than cytokines during CCl4-induced fibrogenesis. Mol Cells 10(3):289–300